Local oceanic precursors for the summer monsoon onset over the Bay Of Bengal and the underlying processes

Article *in* Journal of Climate · June 2016

DOI: 10.1175/JCLI-D-15-0825.1

CITATIONS
2

READS
108

4 authors, including:

Jianping Li
Ocean University of China
490 PUBLICATIONS **9,161** CITATIONS
SEE PROFILE

Xingwen Jiang
Institute of Plateau Meteorology, China Meteorological Administration
38 PUBLICATIONS **404** CITATIONS
SEE PROFILE

Local Oceanic Precursors for the Summer Monsoon Onset over the Bay of Bengal and the Underlying Processes

NAN XING

College of Global Change and Earth System Science, Beijing Normal University, Beijing Meteorological Observatory, and Joint Center for Global Change Studies, Beijing, China

JIANPING LI

College of Global Change and Earth System Science, Beijing Normal University, and Joint Center for Global Change Studies, Beijing, China

XINGWEN JIANG

Institute of Plateau Meteorology, China Meteorological Administration, Chengdu, Sichuan, China

LANNING WANG

College of Global Change and Earth System Science, Beijing Normal University, and Joint Center for Global Change Studies, Beijing, China

(Manuscript received 19 November 2015, in final form 30 March 2016)

ABSTRACT

Local sea surface temperature (SST) plays an important role in the onset of the Bay of Bengal (BoB) summer monsoon (BoBSM). Previous study indicated that the meridionally warmest SST axis (WSSTA) appears in mid-April in the central BoB, which may be a precursor for the BoBSM onset. In this study, it is found that a warm but not the meridionally warmest center, which is defined as the secondary WSSTA (SWSSTA), occurs in early April in the central BoB, leading the BoBSM onset by five pentads. Dates of the SWSSTA occurrence are significantly positively correlated with dates of the WSSTA occurrence in the central BoB and the BoBSM onset on an interannual time scale. The SWSSTA is an earlier precursor for the BoBSM onset. The formation of the oceanic precursor and its impact on the BoBSM onset are as follows. Before the BoBSM onset, resulting from more surface heat input and shallower mixed layer affected by the low-level anticyclone and subtropical high in the central BoB, local SST shows the most rapid increase. Meanwhile, the situation is adverse to the rapid increase of SST in the equatorial BoB. For this reason, the SWSSTA occurs, and the WSSTA subsequently appears in the central BoB. The WSSTA in turn enhances local convection, eliminates the low-level anticyclone, and moves the subtropical high outward away from the BoB by inducing atmospheric instability, thus developing a heating center. Convectional heating further strengthens southwesterlies in the BoB by exciting mixed planetary–gravity waves, resulting in the BoBSM onset.

1. Introduction

Monsoon onset is the most important subseasonal variation of monsoons (Webster et al. 1998; Jiang and Li 2011); it is characterized by the start of the rainy season, large-scale convection, and an abrupt change in atmospheric circulation (Li and Zhang 2009). The Asian monsoon is the archetypal monsoon system and has been investigated from various perspectives (e.g., Roxy and Tanimoto 2007; Fu et al. 2013; Jiang et al. 2013a,b). Previous studies have reported that the onset of the Asian summer monsoon occurs first over the Bay of Bengal (BoB), then over the South China Sea (SCS), and finally over India, despite differences in data and definitions of monsoon onset (e.g., Wu and Zhang 1998; Mao et al. 2002; Mao 2002; Wang and LinHo 2002; Li and Zhang 2009). Associated with the BoB summer

Denotes Open Access content.

Corresponding author address: Dr. Jianping Li, Professor, College of Global Change and Earth System Science, Beijing Normal University, 19 XinJieKouWai St., Beijing 100875, China.
E-mail: ljp@bnu.edu.cn

DOI: 10.1175/JCLI-D-15-0825.1

monsoon (BoBSM) onset, local convective activity has an important influence on the subsequent monsoon onset over the SCS and Indian Ocean by changing atmospheric circulation patterns over these regions (Liu et al. 2002; Tamura and Koike 2010). Moreover, anomalies in the BoBSM onset timing are also closely related to rainfall anomalies in southwestern China (Yan et al. 2003; Chen et al. 2006). Therefore, the timing of the BoBSM onset plays an important role in the timing of the subsequent monsoon onset and the climate over local and remote regions.

Some studies have focused on understanding the BoBSM onset in terms of land–sea thermal contrast and emphasized the role of land heating. He et al. (1987) indicated that reversal of the meridional temperature gradient in the upper troposphere induced by northward displacement of the South Asian anticyclone changes meridional circulation and leads to the onset of the Southeast Asian monsoon. Yanai et al. (1992) found similar results, but indicated that the reversal of the meridional temperature gradient in the upper troposphere results from the sensible heat flux from the surface of the Tibetan Plateau. Wu and Zhang (1998) showed that thermal and mechanical forcing by the Tibetan Plateau favors the Asian summer monsoon onset that occurs first over the BoB.

In addition to the role of land heating, variation of local sea surface temperature (SST) plays an important role in monsoon onset over the BoB. Wu et al. (2010, 2012) found in two case studies that the vortex induced by warm SST over the BoB triggers the BoBSM onset. Previous studies also pointed out that warm SST could induce the northward movement of the intraseasonal oscillation (ISO) by enhancing the unstable condition, thus triggering the monsoon onset (Li et al. 2013, 2015; Zhou and Murtugudde 2014). Using reanalysis data, Jiang and Li (2011) also found that the meridional SST gradient associated with the occurrence of the meridionally warmest SST axis (WSSTA) in the central BoB may be a precursor for the BoBSM onset. This relationship was further confirmed by Yu et al. (2012) using in situ buoy data. However, the year-to-year variations of the relationship between the WSSTA occurrence in the central BoB and the monsoon onset are unclear. Moreover, the WSSTA occurrence in the central BoB is only about two pentads earlier than the monsoon onset (Jiang and Li 2011). It thus remains to be found whether there are monsoon onset precursors that occur before the WSSTA occurrence in the central BoB. If so, what are the possible reasons for the occurrence of the precursors and the physical mechanisms linking the precursors and the BoBSM onset?

Although previous studies show that the climatological BoBSM onset is closely related to the variation of local SST (Jiang and Li 2011; Yu et al. 2012), they do not give a dynamic explanation for the way in which SST patterns affects monsoon onset as well. Considering that tropical SST is closely related to atmospheric heating (Yanai and Tomita 1998; Jian et al. 2004; Lan et al. 2005), which plays an important role in driving tropical circulation (Lorenz 1955; Webster 1972), a simple theoretical model (Gill 1980; Xing et al. 2014) is used to verify the possible link between oceanic precursors and the BoBSM onset.

The remainder of this paper is organized as follows. In section 2, we describe the data and analytical methods used in this study. In section 3, we depict the climatological annual cycle of SST and wind in the lower troposphere over the BoB using a quantitative definition of the WSSTA anew, in order to describe the temporal and spatial variations of the WSSTA and find new oceanic precursors. In section 4, we analyze the physical processes associated with the formation of the oceanic precursors before the BoBSM onset. In section 5, the role of the oceanic precursors in the BoBSM onset is investigated. A summary of the results and further discussion are provided in section 6.

2. Data and methodology

a. Data

Daily wind, geopotential height, temperature, specific humidity, and total cloud cover data used in this study were derived from the National Centers for Environmental Prediction–National Center for Atmospheric Research (NCEP–NCAR) reanalysis (Kalnay et al. 1996), with a horizontal resolution of 2.5 × 2.5° covering the period 1982–2010. Objectively analyzed air–sea fluxes (OAFlux) with a horizontal resolution of 1° × 1° are used for the period 1985–2009 (Yu and Weller 2007; Yu et al. 2008). Daily outgoing longwave radiation (OLR) was provided by the National Oceanic and Atmospheric Administration (NOAA) Climate Diagnostics Center (CDC) (Liebmann and Smith 1996), with a horizontal resolution of 2.5° × 2.5° for the period 1982–2010. Pentad precipitation is based on the Climate Prediction Center (CPC) Merged Analysis of Precipitation (CMAP), available on a 2.5° grid (Xie and Arkin 1997). Daily SST data are from the NOAA optimum interpolation (OI) analysis (Reynolds et al. 2007), with a horizontal resolution of 0.25° × 0.25° for the period 1982–2010. Mixed layer depth data for the period 1982–2010 are from the NCEP Global Ocean Data Assimilation System (GODAS) (Derber and

Rosati 1989; Behringer et al. 1998), with a resolution of $1° \times 0.333°$ in longitude and latitude, respectively, and a 5-day (one pentad) time resolution. The SST data were averaged to a resolution of $1° \times 1°$ to remove small-scale disturbances. All daily time series were smoothed using a 5-day running average.

b. Methodology

Jiang and Li (2011) defined the possible precursor WSSTA for the BoBSM onset as the meridional SST maximum in the tropical ocean. Based on the physical concept, the corresponding quantitative definition is given in this study. A local maximum SST meets the following two criteria. First, the first derivative of SST with respect to y is equal to zero (i.e., $\partial T/\partial y = 0$). Second, the second derivative of SST with respect to y is less than zero (i.e., $\partial^2 T/\partial y^2 < 0$). Thus, the meridional SST maximum $T_{\max}$ is selected from all positions that meet the first two criteria in the tropical ocean. The boundary condition is such that if the SST on the boundary T_b is higher than $T_{\max}$, that is $T_b > T_{\max}$, then $T_{\max} = T_b$, and $T_{\max}$ is defined as the WSSTA. Apart from the WSSTA, we further define the secondary WSSTA (SWSSTA) as a local SST maximum.

We use three indices to characterize the interannual variation in the BoBSM onset, which are based on OLR, 925-hPa zonal wind U (Jiang 2011), and the meridional mean temperature gradient (MTG) in the middle and upper troposphere from 500 to 200 hPa (Mao 2002). Based on OLR, the BoBSM onset date is defined as the first day after 1 April on which the average OLR over 5°–15°N, 85°–95°E is less than 230 W m^{-2} in the following seven days (including the first day). Based on U, the BoBSM onset date is defined as the first day after 1 April on which the average 925-hPa zonal wind over 2.5°–10°N, 80°–95°E is more than 3.0 m s^{-1} in the following seven days (including the first day). The BoBSM onset date based on MTG is defined as the first day after 1 April that satisfies the following two criteria: 1) the areal mean of MTG over 5°–15°N, 85°–95°E is more than 0 K m^{-1}; 2) in the following nine days, the areal mean MTG is more than 0 K m^{-1} on at least six days.

The method for locating the subtropical high ridge was elaborated by Li and Chou (1998) and Zhan et al. (2005). The characteristic line with zonal wind $u = 0$ and $\partial u/\partial y > 0$ over subtropical areas is used to identify the subtropical ridge. In the same way, the meridional ridge is identified by the characteristic line with meridional wind $v = 0$ and $\partial v/\partial x < 0$. The intersection of zonal and meridional ridges is defined as the center of the anticyclone, and the geopotential height of the center is defined as the intensity of the anticyclone in the lower troposphere.

A simple mixed-layer model will be used to analyze SST variation in this study. Assuming that the temperature and velocity are uniform over the mixed layer, the temperature equation for the mixed layer is as follows (McPhaden and Hayes 1991; Huang et al. 2010):

$$\begin{aligned}
&\frac{\partial T}{\partial t} = Q_n/\rho_0 C_P h = (Q_0 + Q_a + Q_e)/\rho_0 C_P h,\\
&Q_0 = Q_{\mathrm{sw}} - Q_{\mathrm{lw}} - Q_{\mathrm{sh}} - Q_{\mathrm{lh}},\\
&Q_a = -\rho_0 C_P h \mathbf{V}_a \cdot \nabla T_a,\\
&Q_e = -\rho_0 C_P h \omega_e (T_a - T_{-h})/h, \quad \text{and}\\
&\omega_e = \partial h/\partial t + \mathbf{V}_{-h} \cdot \nabla h + \omega_{-h},
\end{aligned} \tag{1}$$

where $\partial T/\partial t$ is the local time rate of temperature change, Q_n is the mixed-layer heat budget, h represents the mixed layer depth (MLD); water density ρ_0 and the heat capacity of water at constant pressure C_P are assumed constant at 10^3 kg m^{-3} and 3.94×10^3 J kg^{-1} °C^{-1}, respectively. The net surface heat flux Q_0 consists of shortwave radiation flux Q_{sw}, longwave radiation flux Q_{lw}, sensible flux Q_{sh}, and latent flux Q_{lh}. The flux induced by horizontal temperature advection in the mixed layer is Q_a, where $\mathbf{V}_a$ and ∇T_a denote the averaged horizontal velocity and horizontal temperature gradient over the mixed layer, respectively. The flux induced by vertical entrainment through the bottom of the mixed layer is Q_e. The difference between temperatures averaged over the mixed layer and the base of the mixed layer is ΔT_{-h}. Entrainment velocity through the base of the mixed layer is ω_e, where ω_e is the sum of the vertical velocity at the base of the mixed layer ω_{-h} and the time rate of change of the mixed-layer thickness, $\partial h/\partial t + \mathbf{V}_{-h} \cdot \nabla h$.

The apparent heat source Q_1 (Yanai et al. 1973, 1992) is defined by

$$Q_1 = C_p (p/p_0)^k (\partial\theta/\partial t + \mathbf{V} \cdot \nabla\theta + \omega \partial\theta/\partial p), \tag{2}$$

where θ is the potential temperature, $\mathbf{V}$ is the horizontal velocity, ω is the vertical pressure velocity, and p is the pressure. In the equation $k = R/C_p$, where R and C_p are the gas constant and the specific heat at constant pressure of dry air, respectively, $p_0 = 1000$ hPa, and ∇ is the isobaric gradient operator. In this study, we integrate Eq. (2) from the tropopause (taken as 100 hPa) to the surface (1000 hPa) to obtain the atmospheric heat source for the whole atmospheric column.

3. Precursors for monsoon onset over the BoB

Figure 1 shows the climatological annual cycle of longitudinally averaged (85°–95°E) SST and 925-hPa

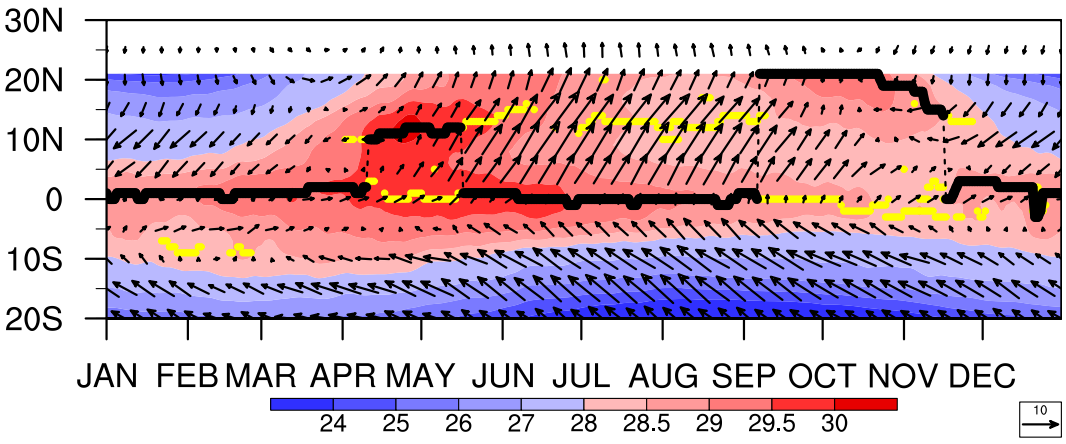

FIG. 1. Latitude–time diagram of climatological longitudinally averaged (85°–95°E) SST (shading; °C) and wind (vectors; m s^{-1}) at 925 hPa over the BoB. The solid black lines represent the WSSTA, and the yellow dots represent the SWSSTA.

wind over the BoB. Two warm SST axes occur in the BoB: one around the equator and the other in the central and northern BoB. The axis around the equator exists year-round, while the axis in the central and northern BoB appears from early April until late November. The locations of the warmest and secondary warmest SST centers vary with season. The WSSTA is stagnant around the equator, except at two periods: 1) the WSSTA occurs around 10°N in mid-April before the onset of the southwesterlies, remains for about a month, and 2) then returns to the equator until it occurs in the northern BoB again in early September (Jiang and Li 2011). The SWSSTA (yellow dots in Fig. 1) appears in early April around 10°N over the BoB, two pentads earlier than the WSSTA occurrence around 10°N. Jiang and Li (2011) and Yu et al. (2012) pointed out that the WSSTA occurrence in the central BoB is a good indicator for monsoon onset. Therefore, the SWSSTA may be an earlier precursor for the BoBSM onset.

To confirm the possible precursors for the monsoon onset, evolutions of pentad-mean SST and 925-hPa wind relative to dates of the BoBSM onset defined by the *U* index (Jiang 2011) are given in Fig. 2. At pentad −6, SST is warmest in the tropics, and the WSSTA is located around the equator. Meanwhile, the SWSSTA occurs first in the east-central BoB, leading the monsoon onset by 5 pentads, and it subsequently spreads in the central BoB during the following 2 pentads, which indicates the rapid SST warming in the central BoB (Figs. 2a–c). Then the WSSTA occurs around 10°N, and an SWSSTA remains in the tropics (Fig. 2d). After the WSSTA appears in the central BoB, southwesterlies gradually develop south of the WSSTA (Figs. 2e,f) and dominate the BoB, indicating summer monsoon onset over the BoB (Fig. 2g). Comparison of the SST patterns over the BoB, the Arabian Sea, and the SCS shows that there is no SWSSTA over the Arabian Sea, and the WSSTA is stagnant and the wind patterns remain essentially constant over the Arabian Sea and SCS before the BoBSM onset. This further suggests that the BoBSM onset is the earliest in the Asian summer monsoon and supports the relationship between occurrences of the SWSSTA and WSSTA in the central BoB and the BoBSM onset.

To identify the relationship between occurrences of the SWSSTA and the WSSTA in the central BoB and the BoBSM onset, we define the SWSSTA occurrence date as the first day after 15 March that satisfies the following criteria: first, the SWSSTA occurs between 6° and 15°N in the BoB; second, the SWSSTA exists for at least 7 of the following 10 days (including the first occurrence day). The WSSTA occurrence is defined as the first day after 1 April that satisfies the following criteria: first, the WSSTA occurs between 8° and 15°N in the BoB; second, the WSSTA exists for at least 7 of the following 10 days (including the first occurrence day).

Dates of the SWSSTA occurrence, the WSSTA occurrence, and the BoBSM onset based on 925-hPa zonal winds (Jiang 2011), OLR, and MTG (Mao 2002) for each individual year are displayed in Fig. 3. The BoBSM onset dates based on different indices show significantly interannual variation, with the range between the earliest and the latest onset dates exceeding 1 month. In most years, occurrence dates of both the SWSSTA and the WSSTA are earlier than the monsoon onset, and the SWSSTA occurs earlier than the WSSTA in the central BoB. It is also seen that the occurrences of the SWSSTA and WSSTA and the monsoon onset based on the three indices vary in phase in most years.

The mean dates of the BoBSM onset are 29 April, 29 April, and 28 April for the three onset indices *U*,

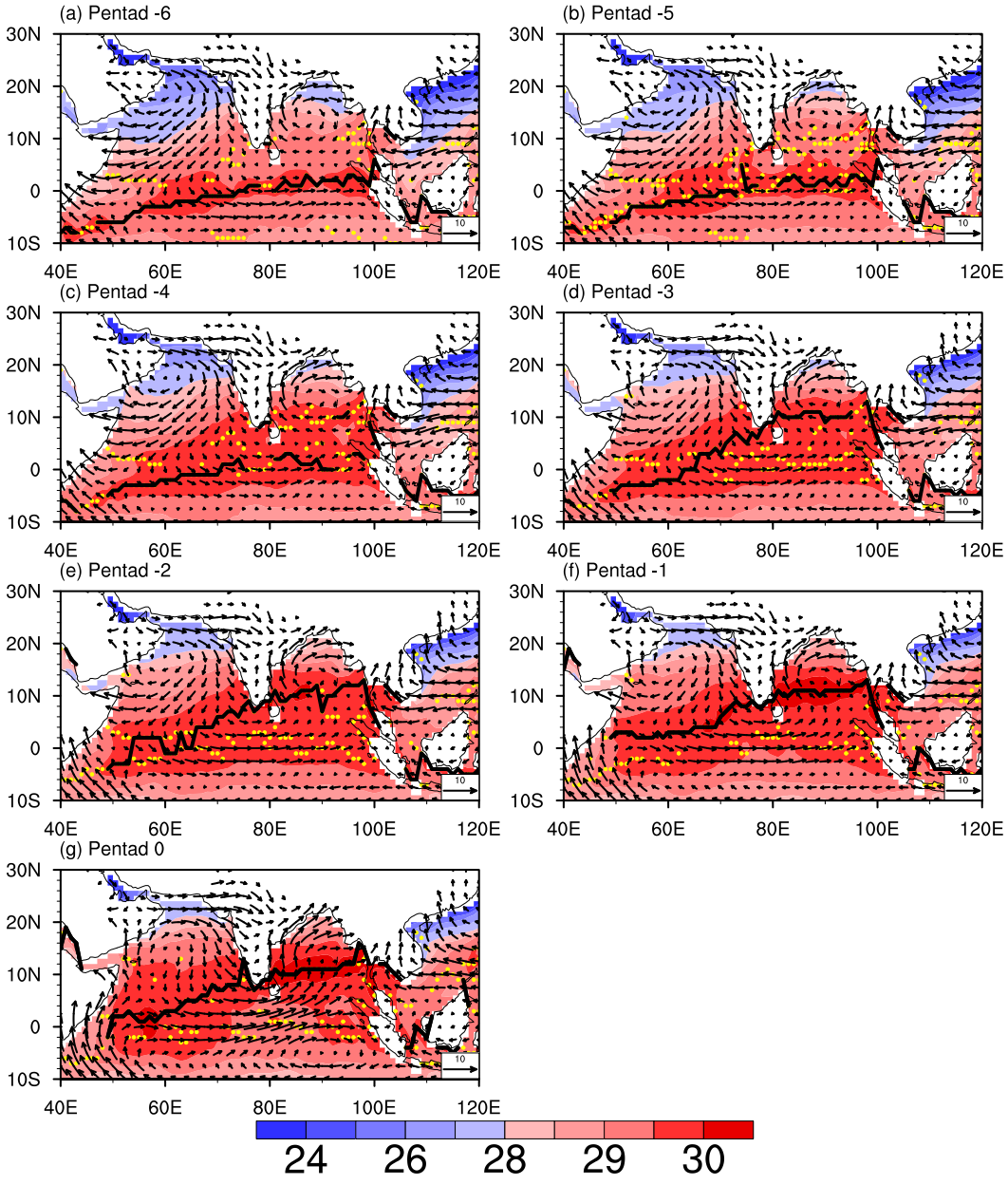

FIG. 2. Composite patterns of pentad-mean SST (shading; °C) and wind (vectors; m s^{-1}) at 925 hPa before the BoBSM onset, with dates of the BoBSM onset taken as the zero pentad. The solid black lines represent the WSSTA, and the yellow dots represent the SWSSTA.

OLR, and MTG, and the values of the standard deviations of the onset indices are 11, 13, and 15 days, respectively. The three monsoon onset indices are significantly correlated with each other, exceeding the 95% confidence level (Table 1). The result is consistent with previous studies, despite some differences in onset indices (e.g., Mao and Wu 2007). The climatological dates of the SWSSTA and WSSTA indices are 30 March and 14 April, with standard deviations of 13 and 10 days, which correspond closely to the climatological dates of the SWSSTA and WSSTA occurrences shown in Fig. 1, respectively. The result indicates that the SWSSTA and the WSSTA indices are effective in characterizing the occurrences of the SWSSTA and the WSSTA. Moreover, the SWSSTA is highly correlated with the WSSTA, with a correlation coefficient of 0.74 at the 99.9% confidence level, and both oceanic precursor indices are highly correlated with the three onset indices, exceeding the 95% confidence level (Table 1).

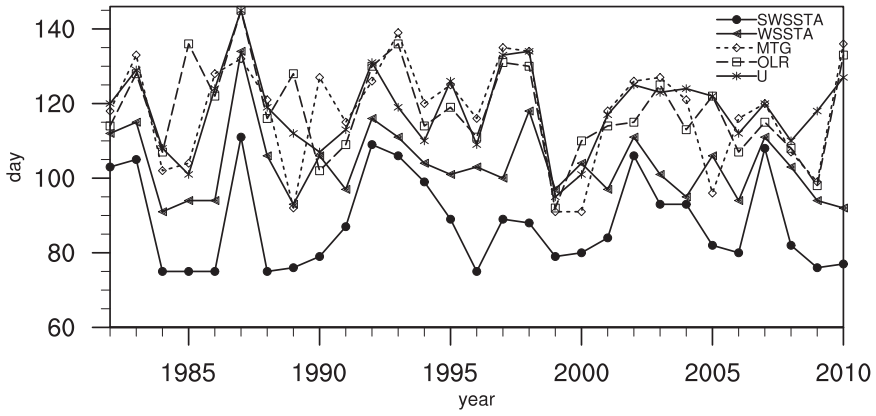

FIG. 3. Time series of the BoBSM onset dates defined by *U* (asterisks), MTG (diamonds), OLR (squares), and dates of the WSSTA (solid triangles) and the SWSSTA occurrences (dots). All dates are Julian days in the calendar year.

To conclude, the SWSSTA appears earlier than the WSSTA, which is followed by the BoBSM onset on climatological and interannual time scales, and the SWSSTA occurrence indices are significantly positively correlated with the WSSTA occurrence and the BoBSM onset indices. Therefore, the SWSSTA occurrence is an earlier precursor for the BoBSM onset than the WSSTA occurrence.

4. The formation of the oceanic precursors

a. Heat budget analysis of the SWSSTA and the WSSTA occurrences in the central BoB

Occurrences of the SWSSTA and the WSSTA in the central BoB indicate uneven warming of SST with latitude before the BoBSM onset. SST variation is closely related to mixed-layer temperature variation (McPhaden and Hayes 1991; Huang et al. 2010), and hence the temperature equation for the mixed layer described by McPhaden and Hayes (1991) and Huang et al. (2010) is used to analyze the variability and controls on SST. To analyze the possible causes of the oceanic precursors, the BoB is divided into three regions: the equatorial BoB (2°S–2°N, 85°–95°E), the southern BoB (3°–7°N, 85°–95°E), and the central BoB (8°S–13°N, 85°–95°E), based on the characteristics of SST distribution before the BoBSM onset in Figs. 1 and 2. Moreover, to better depict the evolution features of meteorological variables associated with the BoBSM onset, all the following time evolution maps are obtained with reference to dates of the BoBSM onset defined by *U* (Jiang 2011).

Pentad-average rates of increase of mixed-layer temperature in the three regions relative to dates of the BoBSM onset are given in Fig. 4a. Before the BoBSM onset, increasing rates of temperature are more than 0°C pentad^{-1}, but with different temporal variation over the three regions. In the central BoB, the rate increases first and decreases after pentad −2, while in the southern and equatorial BoB, it rarely increases and decreases after pentad −5. In general, mixed-layer temperature increases most rapidly in the central BoB before the BoBSM onset, followed by the southern BoB, and finally the equatorial BoB. The most rapid rate of increase in the central BoB contributes to the local warm center and hence results in occurrences of the SWSSTA and the WSSTA prior to the BoBSM onset (Fig. 1 and 2). At the equator, SST increases slowly; meanwhile, the increasing rates for SST scarcely vary with latitude during the BoBSM onset (figures not shown). Therefore, it is seen that an SWSSTA sustains in the equatorial BoB even though the WSSTA appears in the central BoB (Fig. 1).

According to Eq. (1), the rate of temperature variation is proportional to the mixed-layer heat budget and inversely proportional to mixed layer depth. Increasing positive rates of SST are due to net mixed-layer heat input in the three regions (Fig. 4). The evolution of the mixed-layer heat budget (Figs. 4b–d) further shows that,

TABLE 1. Correlation coefficients between dates of the SWSSTA and WSSTA occurrence in the central BoB and the BoBSM onset based on *U*, MTG, and OLR indices. Values denoted with one, two, three, and four asterisks exceed the confidence levels of 95%, 99%, 99.5%, and 99.9%, respectively.

	U	MTG	OLR	WSSTA	SWSSTA
U	1				
MTG	0.71****	1			
OLR	0.65****	0.53***	1		
WSSTA	0.57***	0.43*	0.43*	1	
SWSSTA	0.56***	0.52***	0.39*	0.74****	1

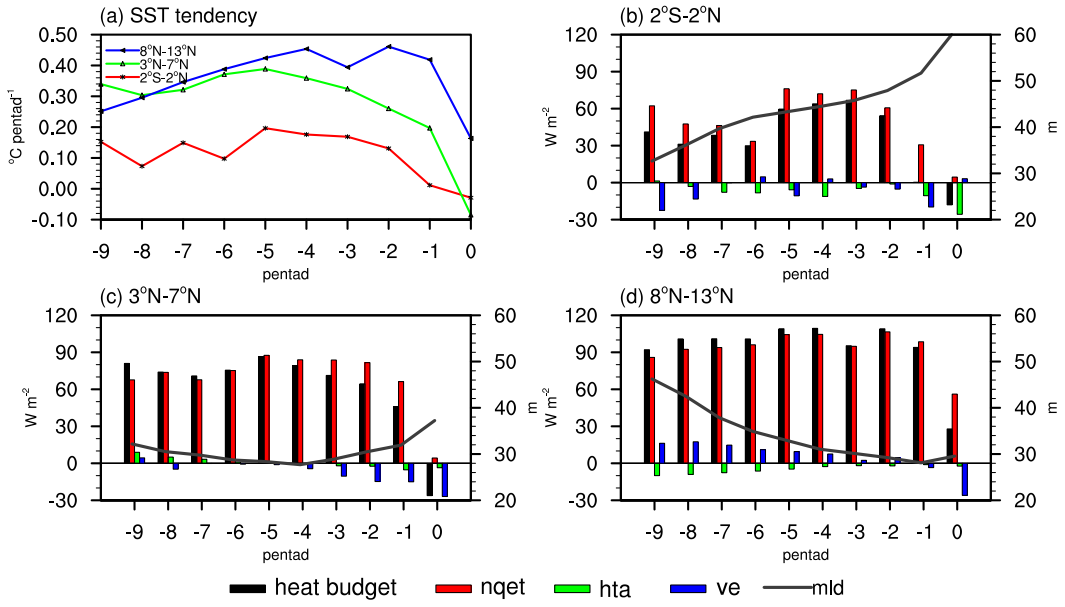

FIG. 4. Evolutions of (a) pentad-mean rate of increase of mixed-layer temperature (°C pentad^{-1}) averaged over the equatorial (2°S–2°N, 85°–95°E; red lines), southern (3°–7°N, 85°–95°E; green lines), and central (8°–13°N, 85°–95°E; blue lines) BoB before the BoBSM onset. Evolutions of pentad-mean mixed-layer heat input (heat budget) (black bars; W m^{-2}), net surface heat flux (nqet) (red bars; W m^{-2}), flux induced by horizontal temperature advection within the mixed layer (hta) (green bars; W m^{-2}) and flux induced by vertical entrainment through the bottom of the mixed layer (ve) (blue bars; W m^{-2}), and MLD (gray lines; m, right *y* axis) in the (b) equatorial, (c) southern, and (d) central BoB before the BoBSM onset. Composites are in reference to dates of the BoBSM onset, which are taken as the zero pentad.

before the BoBSM onset, net mixed-layer heat input increases first and decreases after pentad −2 in the central BoB, while it has a rare increasing trend before pentad −5 in the equatorial and southern BoB, but suddenly increases hereafter and then decreases in both regions. As a whole net mixed-layer heat input is most in the central BoB, followed by the southern BoB, and finally by the equatorial BoB. Meanwhile, the mixed layer gradually shoals (deepens) in the central (equatorial) BoB, while in the southern BoB, it shoals first and deepens after pentad −4. After the WSSTA occurrence, the mixed layer shoals gradually from the tropical to central BoB. Thus, the combined action of the two factors is favorable to the most rapid increase of SST in the central BoB (Figs. 1 and 2), which is consistent with previous results (Wu et al. 2012). Moreover, as mentioned above, the SWSSTA and WSSTA do not occur in the central Arabian Sea during the same period (Fig. 2). Some studies indicated that the mixed layer is deeper in the Arabian Sea than in the BoB during the same period (Roxy et al. 2013), and it is shallower in the equatorial BoB than in the central Arabian Sea (Kumar and Narvekar 2005), which does not favor the rapid increase of SST in the Arabian Sea and the development of a warm center in the central Arabian Sea. In other words, the distribution differences of mixed layer depth between the BoB and Arabian Sea may result in different SST patterns before the BoBSM onset.

As shown in Eq. (1), the mixed-layer heat budget includes the net surface heat flux, fluxes of horizontal advection, and vertical entrainment. In the three regions, net surface heat fluxes are observed to be in phase with the mixed-layer heat input, while the other fluxes vary differently (Figs. 4b–d). Around the equator, cold water upwelling weakens first and enhances after the occurrence of the SWSSTA, and cold advection enhances as a whole prior to the BoBSM onset, together opposing the increase of the mixed-layer heat budget (Fig. 4b). In the southern BoB, cold water upwelling enhances as a whole, and the flux induced by horizontal advection reverses from positive to negative before the BoBSM onset, together reducing the mixed-layer heat budget (Fig. 4c). In the central BoB, negative flux from cold advection and positive flux induced by vertical entrainment decrease with time before the BoBSM onset, which together favor the increase of the mixed-layer heat budget (Fig. 4d). However, upon comparison of each component of the mixed-layer heat budget in the three regions, fluxes induced by horizontal advection and vertical entrainment are small in comparison. This

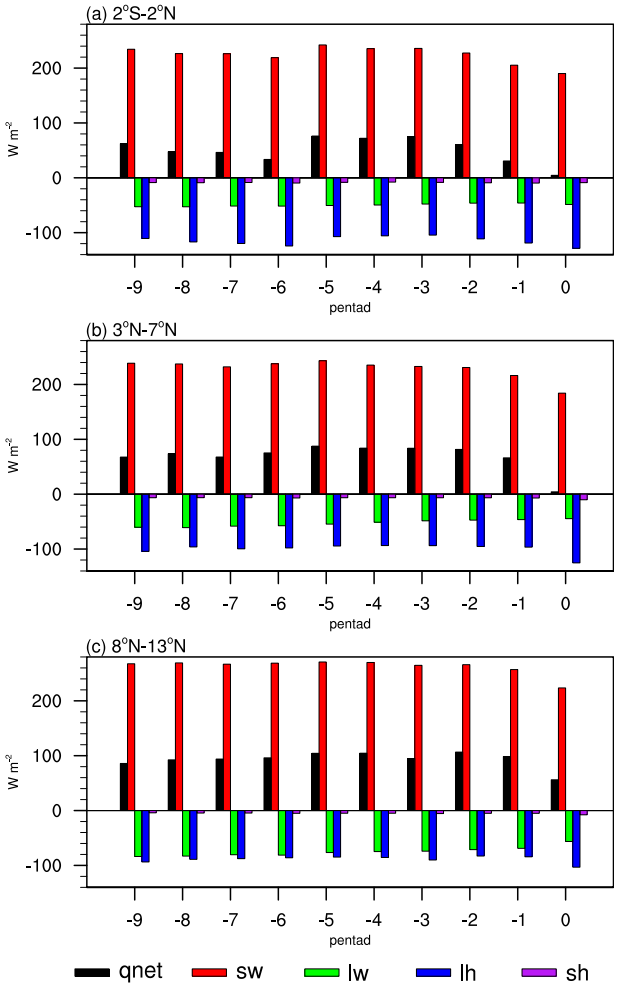

FIG. 5. (a)–(c) As in Figs. 4b–d, but for qnet (black bar; $W m^{-2}$), downward shortwave radiation heat flux (sw) (red bars; $W m^{-2}$), upward longwave radiation heat flux (lw) (green bars; $W m^{-2}$), latent heat flux (lh) (blue bars; $W m^{-2}$), and sensible heat flux (sh) (purple bars; $W m^{-2}$). Positive flux means surface uptake.

suggests that net surface heat flux mainly contributes to the mixed-layer heat input.

To further analyze the factors influencing net surface heat flux, pentad-average composites for the downward shortwave radiation flux, longwave radiation flux, latent heat flux, and sensible heat flux, which are the main components of net surface heat flux relative to dates of the BoBSM onset, are shown in Fig. 5. Variation of the downward shortwave radiation flux are consistent with net surface heat flux in the three regions, and the downward shortwave radiation flux in the central BoB is more than in the equatorial and southern BoB. The longwave radiation flux and latent and sensible heat fluxes oppose the shortwave radiation flux, reducing net surface heat flux in the three regions. Among them, the longwave radiation flux decrease with time in the three regions before the BoBSM onset, and it is greatest in the central BoB, followed by the southern BoB, and finally by the equatorial BoB. Latent heat flux increases first and decreases after pentad −6, then increases after pentad −3 in the equatorial BoB, while it decreases first and increases about after pentad −4 (−3) in the southern (central) BoB. Meanwhile, latent heat flux in the central BoB is less than in the southern and equatorial BoB. Sensible heat flux opposes net surface heat flux in the BoB, but it differs rarely in the three regions, and it is relatively small in comparison. To sum up, more shortwave radiation flux and less latent flux together result in more net surface heat flux in the central BoB than in the equatorial and southern BoB.

From the point of view of the heat budget, we find that, before the BoBSM onset, meridional variation of the mixed-layer heat input and the mixed layer lead to the occurrences of the SWSSTA and the WSSTA in the central BoB. Moreover, the most important contributor to variation of the mixed-layer heat budget is net surface heat flux, which mainly depends on downward shortwave radiation flux and latent heat flux. The main factors affecting downward shortwave radiation flux are solar radiation at the top of the atmosphere and clouds. Solar radiation at the top of the atmosphere varies with the seasonal march of solar heating, and it increases by about $7 W m^{-2}$ in the central BoB from before the occurrence of the SWSSTA (late March) to before the WSSTA occurrence in the central BoB (early April), while the increasing maximum value of downward shortwave radiation flux is about $15 W m^{-2}$ in this period. Moreover, differences in solar radiation at the top of the atmosphere between the central and equatorial BoB are less than $15 W m^{-2}$ since late March–early April (figures not shown), which does not fully explain the difference (about $40 W m^{-2}$) in downward shortwave radiation flux between the central and equatorial BoB in the same period (Fig. 5). The variation of clouds is closely related to atmospheric circulation, and variations of both latent heat flux and mixed layer depth (Fan et al. 2010) are closely related to surface wind speed. Thus, in the next section, we further explore the impact of atmospheric circulation on net surface heat flux and feedback from the net surface heat flux to the atmospheric circulation.

b. *The impact of atmospheric circulation on the heat budget and associated interactions*

Note that an anticyclone appears at 925 hPa over the northwestern BoB before the BoBSM onset (Fig. 2). The anticyclone center moves from the northern BoB to the central BoB with gradually weakened intensity until pentad −3 and subsequently disappears (Figs. 6a,b). In

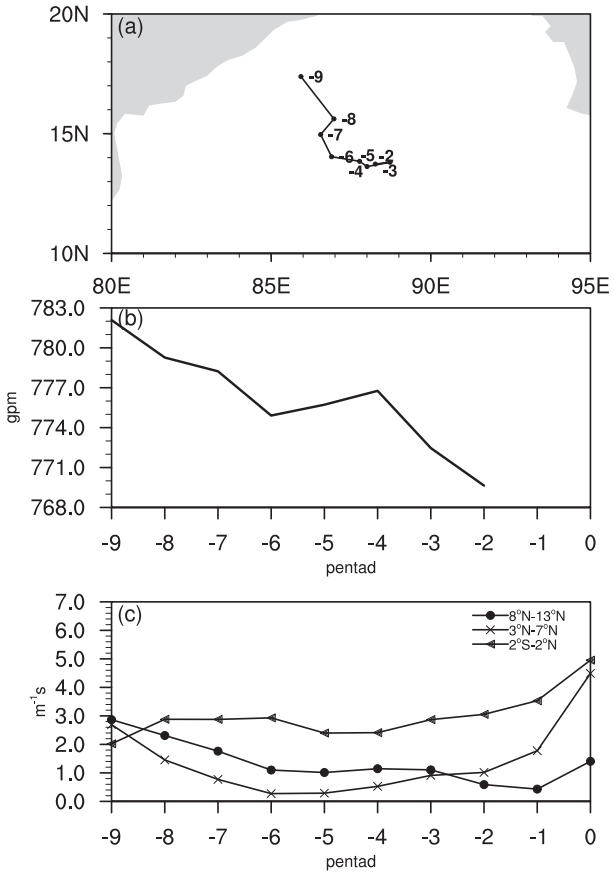

FIG. 6. Evolutions of pentad-mean (a) path, (b) strength of the low-level anticyclone using geopotential height at 925 hPa (gpm), and (c) 925-hPa wind speeds (m s^{-1}) averaged over the equatorial (solid triangles), southern (crosses), and central (dots) BoB before the BoBSM onset, with dates of the BoBSM onset taken as the zero pentad. The path in (a) is labeled with pentad numbers.

the central BoB, the evolution of low-level wind speed is affected by the anticyclone before pentad −3 and also shows a decreasing trend. Low-level wind speed shows an increasing trend as a whole at the equator, while it first decreases and then increases in the southern BoB after pentad −6 (Fig. 6c). In general, low-level speed is the greatest at the equator, and it is greater in the central than in the southern BoB before pentad −3; after that, the situation is reversed.

As the anticyclone moves toward warm SST, warm SST reduces anticyclonic intensity by enhancing atmospheric instability and convergence in the boundary layer (Roxy and Tanimoto 2007) until the anticyclone disappears. Meanwhile, wind speed around the equator attributed to the enhanced surface westerlies is associated with local increasing SST. Surface wind speed is positively related to both latent heat flux and mixed layer depth (Fan et al. 2010), so variation of low-level wind speed is consistent with latent heat flux and mixed layer depth in the three regions, showing more (less) latent heat flux and deeper (shallower) mixed layer in the equatorial (central) BoB as a whole, further favoring the most rapid increase of SST in the central BoB. Thus, there is a positive feedback between SST in the central BoB and low-level wind speed until pentad −3. On one hand, as the anticyclone moves southeastward, warm SST reduces anticyclonic intensity by enhancing instability and convergence in the boundary layer; on the other hand, decreasing wind speed further results in reduced evaporative cooling, as shown by less latent heat flux and mixed layer depth in the central BoB, favoring the increase of local SST (Fig. 6c). This positive feedback between SST and the anticyclone favors a rapid increase of SST until the occurrence of WSSTA in the central BoB.

Anticyclones also occur in the middle troposphere (Fig. 7). Before the BoBSM onset, the subtropical ridge is generally located between 10° and 15°N in the Northern Hemisphere, and it occurs around 13°N over the BoB. Meanwhile, the western Pacific subtropical high (WPSH) and the Indian Ocean subtropical high (IOSH) are located either side of the BoB. Owing to strong downdrafts around the ridge (Fig. 8b), total cloud cover is lower in the central BoB than in the equatorial and southern BoB (Fig. 8a), which corresponds well to downward shortwave radiation flux in the three regions (Fig. 5).

In addition, the WPSH and IOSH move toward the BoB until pentad −3 (Figs. 7a–f). After that, the WPSH and IOSH retreat in opposite directions over the BoB (Figs. 7g–i). Previous studies indicated that increase of SST uplifts local isobaric surface, favoring the extension of subtropical high (Qian et al. 2002). Thus, there exists an interaction between SST and subtropical high. Increase of SST in the central BoB enhances local subtropical high and moves the subtropical high toward the BoB. Meanwhile, the enhanced subtropical high could further decrease cloudiness by suppressing vertical motions and then increase downward shortwave radiation flux, favoring the increase of SST in the central BoB (Figs. 7a–c). After pentad −6, the impact of warm SST on vertical motions overcomes the impact of the subtropical high in the central BoB (Fig. 8b), which increases local cloudiness (Fig. 8a). Because of the increase of local cloudiness, downward shortwave radiation flux slightly decreases in the central BoB, but this does not affect the most rapid increase of SST in the central BoB, so the WPSH and IOSH still move toward the BoB until pentad −3. In the equatorial BoB, variation of vertical motion is mainly influenced by the movements of the WPSH and IOSH, so the total cloud cover decreases first

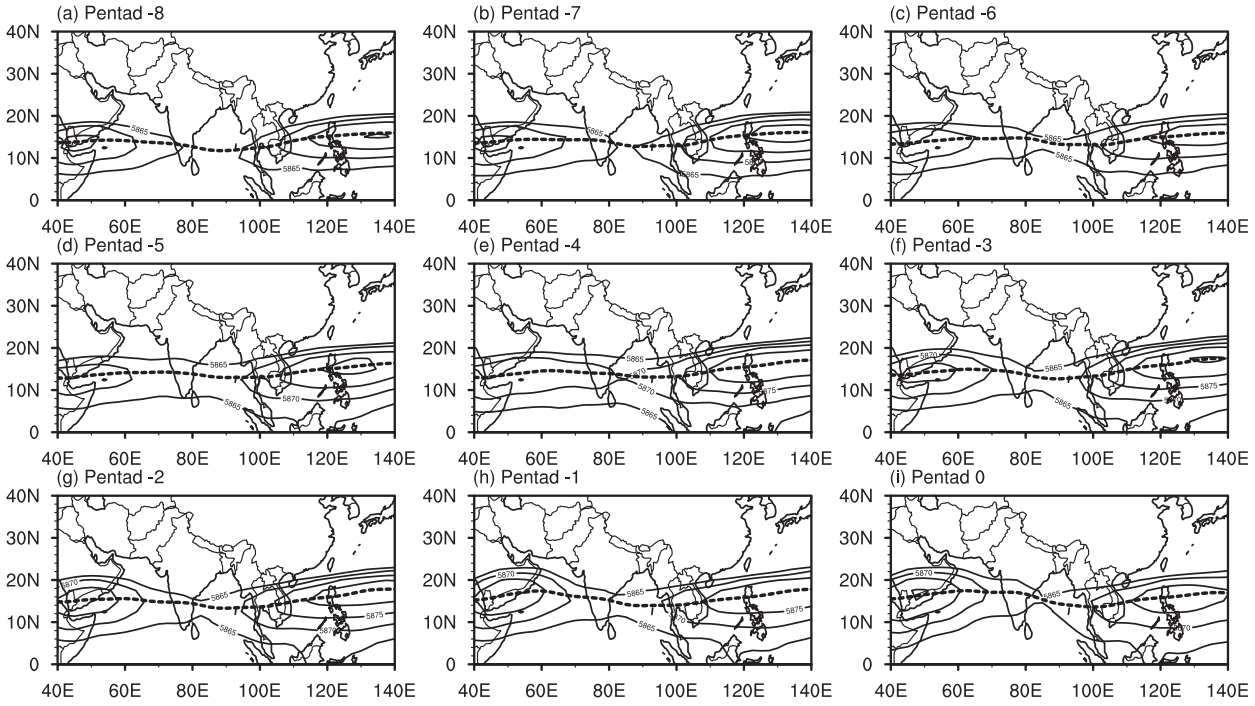

FIG. 7. Composite patterns of pentad-mean geopotential height (gpm) at 500 hPa before the BoBSM onset, with dates of the BoBSM onset taken as the zero pentad. The thick dashed line denotes the position of the subtropical ridge.

and increases after pentad −2 (Fig. 8). Variation of total cloud cover is not exactly consistent with downward shortwave radiation flux in the equatorial BoB, which is possibly due to the decreasing solar radiation at the top of the atmosphere (figure not shown). Thus, besides the seasonal march of solar heating, the seasonal variation of the subtropical high is also favorable to the increase of downward shortwave radiation flux and hence promotes a rapid increase of SST in the central BoB.

5. Role of the WSSTA in the central BoB in triggering the monsoon onset

As mentioned above, after the occurrence of the WSSTA in the central BoB, low-level anticyclones disappear, the WPSH and IOSH move outwards from the BoB, and 2 pentads later the BoBSM subsequently occurs. How does warm SST influence these circulation variations? To clarify the corresponding process, the evolution of surface (1000 hPa) equivalent potential temperature θ_e that measures SST in affecting the atmospheric instability is examined (Fig. 9). As can be seen, the atmospheric unstable condition decreases from the tropical to central BoB before pentad −6. And after that the atmospheric unstable condition is enhanced by the increase of SST in the central BoB, appearing stronger over the north than the south (Li et al. 2015), which favors local gradually enhanced convective activities.

Further, evolutions of pentad-mean OLR, precipitation, and apparent heat source relative to dates of the BoBSM onset are given in Fig. 10. At pentad −3, because of increasing atmospheric instability induced by

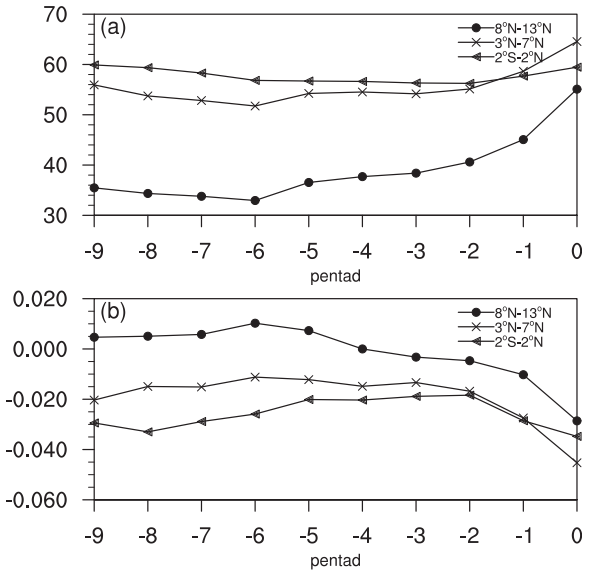

FIG. 8. Evolutions of pentad-mean (a) total cloud cover (%) and (b) vertical velocity at 500 hPa (Pa s^{-1}) averaged over the equatorial (solid triangles), southern (crosses), and central (dots) BoB before the BoBSM onset, with dates of the BoBSM onset taken as the zero pentad.

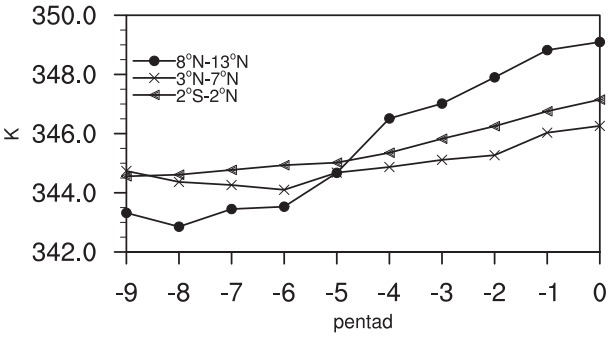

FIG. 9. Evolution of surface (1000 hPa) equivalent potential temperature (K) averaged over the equatorial (solid triangles), southern (crosses), and central (dots) BoB before the BoBSM onset, with dates of the BoBSM onset taken as the zero pentad.

the warm SST, as shown in Fig. 9 (Roxy and Tanimoto 2007), convective activities enhance in the central BoB, giving rise to light precipitation. That is the reason why low-level anticyclones disappear and the WPSH and IOSH moves outwards from the BoB. Meanwhile, one maximum atmospheric heat source's center appears in the central BoB. It is seen that the third term from Eq. (2), $C_p(p/p_0)^k\omega\partial\theta/\partial p$, for the atmospheric heat source is consistent with the atmospheric heat source in the BoB (Figs. 10a and 11a), indicating that the vertical advective term is the main contributor of atmospheric heat sources. Then, owing to local gradually enhanced convective activities, atmospheric heat sources continue to increase in the central BoB before the BoBSM onset, as does precipitation (Figs. 10b,c and 11b,c). In addition, weak southerlies converge toward the southern flank of the WSSTA before the BoBSM onset (Figs. 10b,c). This suggests that strong convective activities induced by the WSSTA could result in a center of atmospheric heat sources in the central BoB before the BoBSM onset. Atmospheric heating is one of the major drivers that directly force the atmospheric circulations (Lorenz 1955; Wang and Qian 2000). Thus, equatorially asymmetric atmospheric heat sources could induce strong southwesterlies in the BoB (Gill 1980) and hence trigger the BoBSM onset (Fig. 10d).

To further confirm the role of atmospheric heat sources in enhancing southwesterlies in the BoB and give the possible dynamic explanation, a simple analytic model (Matsuno 1966; Gill 1980) is used in the present study. Moreover, considering that the pattern of atmospheric heat sources is asymmetric about the equator in the BoB, the general solutions for isolated equatorially asymmetric heating of this model are used in this study (Xing et al. 2014).

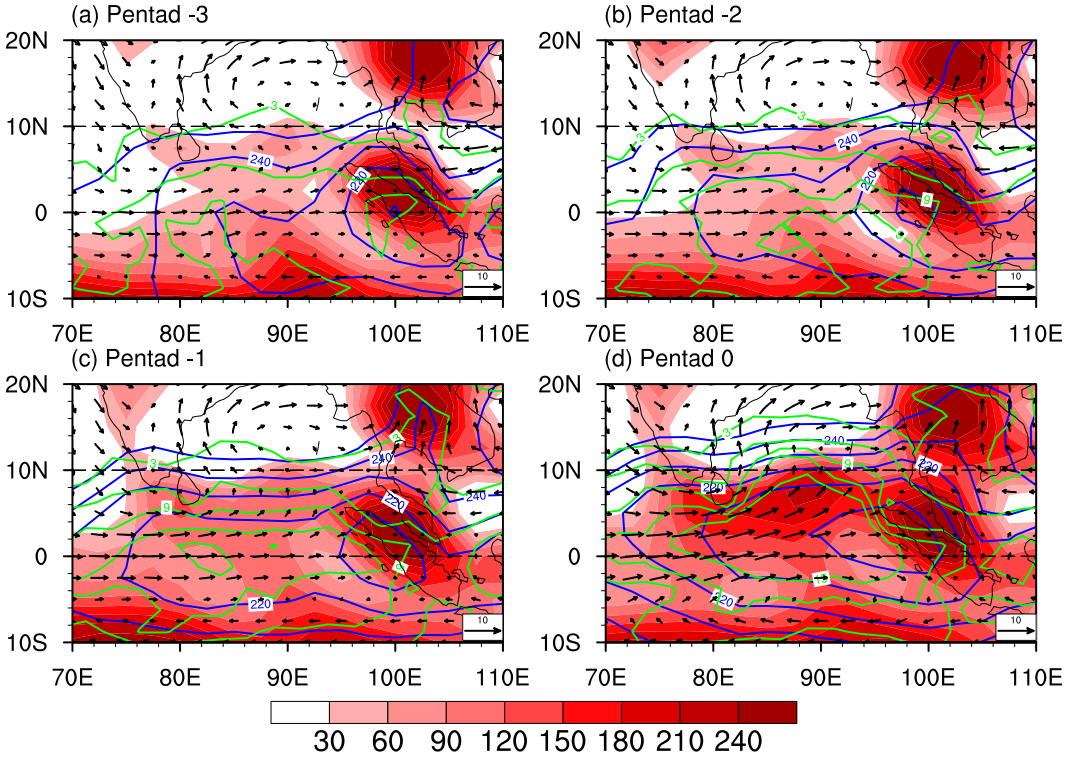

FIG. 10. Composite patterns of pentad-mean precipitation (green contours; mm day^{-1}), OLR (blue contours; W m^{-2}), and apparent heat sources (shading; W m^{-2}) vertically integrated from 1000 to 100 hPa before the BoBSM onset, with dates of the BoBSM onset taken as the zero pentad.

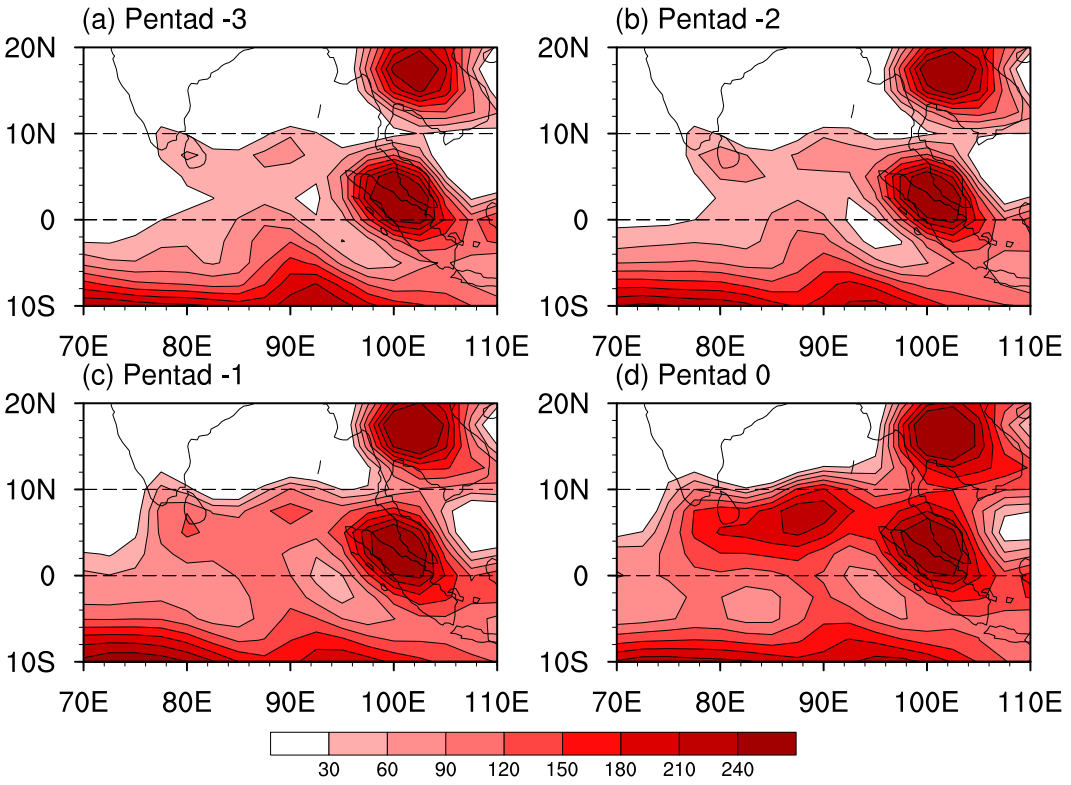

FIG. 11. As in Fig. 10, but only for the third term of Eq. (2), $C_p(p/p_0)^k\omega\partial\theta/\partial p$, for apparent heat sources.

The forcing source used in this study is of the same type as that chosen by Xing et al. (2014), consistent with the form of the WSSTA, with strength decreasing from the center to the surroundings. Figure 12 shows the distribution of the initial ideal heating field. The warm centers are set at the equator (Fig. 12a), 10°N (Fig. 12b), and 10°S (Fig. 12c), reflecting the variation in position of the WSSTA and the corresponding atmospheric heat sources, among which the equatorially symmetric heating has the same form as in Gill (1980). Analytical solutions to the forcing (Gill 1980; Xing et al. 2014) are given in Fig. 13. Compared with the atmospheric response to the equatorially symmetric heating (Fig. 13a), there is no longer a symmetric atmospheric response about the equator, owing to an equatorially asymmetric Rossby wave forced by equatorially asymmetric heating (Figs. 13b,c). The cyclonic circulation in the Northern (Southern) Hemisphere in Fig. 13b (Fig. 13c) strengthens and move northward (southward) compared with that in Fig. 13a, while the cyclonic circulation weakens in the other hemisphere, as does vertical velocity. Cross-equatorial flows from the southwest (northwest) associated with mixed planetary–gravity waves blow along the meridional heat gradient over the region of equatorially asymmetric heating in Fig. 13b (Fig. 13c). Thus, strong southwesterlies are the response of mixed Rossby–gravity waves to equatorially asymmetric heating associated with the WSSTA occurrence in the central BoB. Comparison of the theoretical solutions and those observed heating and wind patterns during the monsoon onset over the BoB indicates that the WSSTA in the central BoB can indeed trigger the monsoon onset process by triggering convection.

6. Conclusions and discussion

We have investigated the interaction between local SST and the BoBSM onset and the evolution of circulation systems associated with the BoBSM onset. Two warm SST axes occur in the BoB: one around the equator and the other in the central and northern BoB. The locations of the SWSSTA and WSSTA vary by season. The SWSSTA in the central BoB appears in early April, 2 pentads earlier than the occurrence of the WSSTA and 5 pentads earlier than the BoBSM onset. Moreover, there is a significant positive correlation between the SWSSTA occurrence and the BoBSM onset, indicating that the SWSSTA is an earlier predictor for BoBSM onset.

Figure 14 shows a schematic of the evolution process of the main atmospheric and oceanic system affecting the BoBSM onset. Since late March (phase I), a low-level

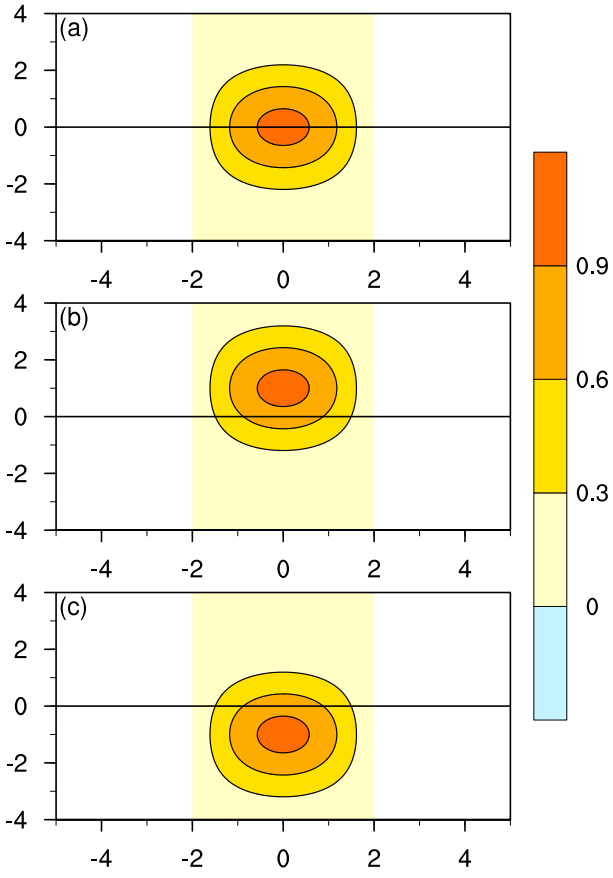

FIG. 12. Distribution of the initial ideal heating for the analytical model: heating center is located (a) at the equator, (b) in the Northern Hemisphere, and (c) in the Southern Hemisphere.

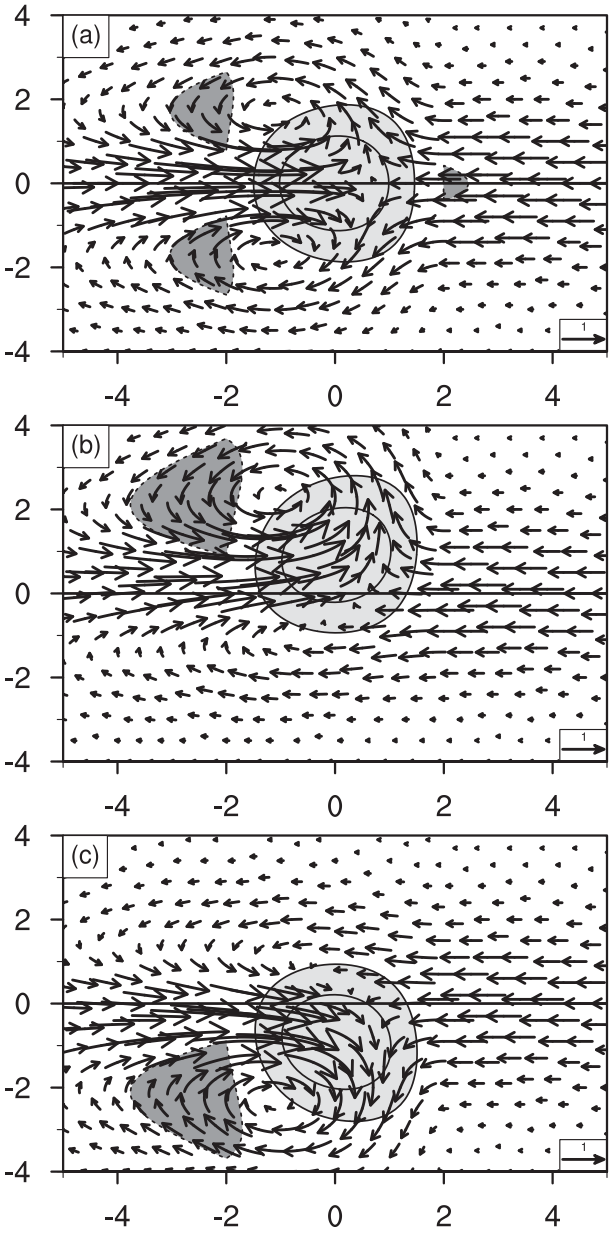

FIG. 13. Horizontal wind (arrows) and vertical velocity (shading) solutions in the lower layer for the isolated heating cases shown in Fig. 12. (a) Analytical solutions for atmospheric variables forced by the heating in Fig. 12a; (b) as in (a), but for Fig. 12b; and (c) as in (a), but for Fig. 12c. The thin solid lines represent ascending flow (light gray shading), with contours of 0.3 and 0.6, while the thin dashed lines represent descending flow (dark gray shading), with contour at −0.1.

anticyclone moves gradually from the northwestern to the southeastern BoB and weakens because of the movement toward warm SST. Meanwhile, the zonal ridge of the subtropical high is located around 13°N over the BoB, and local subtropical high increases as the WPSH and IOSH move toward the BoB. The weakened low-level anticyclone gradually decreases latent heat flux and shoals the mixed layer; the subtropical high favors reducing cloud and increasing surface shortwave radiation flux in the central BoB, resulting in the most rapid increase of SST in the central BoB. For this reason, the SWSSTA occurs, and the WSSTA subsequently appears in the central BoB. Then (phase II) because of increasing atmospheric instability induced by warm SST, the WSSTA triggers a local maximum of convection and leads to the disappearance of the low-level anticyclone and the outward movement of the subtropical high from the BoB. Then the convectional heating in turn strengthens southwesterlies over the BoB by inducing mixed planetary–gravity waves, resulting in the BoBSM onset.

In this study, we have investigated the relationships of the SWSSTA, the WSSTA, and the BoBSM onset and find a good predictive signal for the BoBSM. Both previous and present results show that the atmosphere lags SST by some time (Roxy et al. 2013). In the present study, the leading time of 5 pentads is only a statistical result based on the observation. However, the impact of SST on the

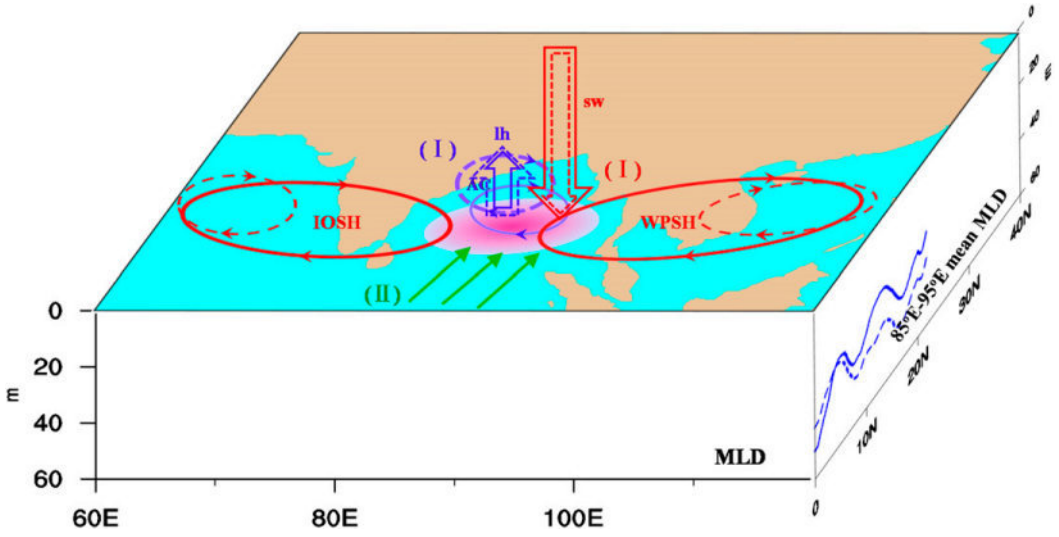

FIG. 14. The schematic diagram showing the evolution process of the main atmospheric and oceanic systems affecting the BoBSM onset: IOSH, WPSH, lh, sw, MLD, and anticyclonic circulation (AC). The pink shading indicates the warming of SST in the central BoB, and green arrows present low-level southwesterlies into the BoB. The main atmospheric and oceanic systems include the IOSH, the WPSH at 500 hPa, the anticyclonic circulation at 925 hPa, and mixed layer depth in the central BoB, respectively. The evolution process of the main atmospheric and oceanic systems affecting the BoBSM onset is divided into two phases from late March to late April. Phase I: the WPSH, IOSH, AC (purple), lh (blue arrows), and sw (red arrows) in the central BoB and mean MLD between 85° and 95°E in the prior period (dashed lines; late March) and late period (solid lines; mid-April); and the most rapid warming in the central BoB associated with phase I. Phase II: low-level southwesterlies (green arrows) induced by the warmest SST in the central BoB resulting from phase I. The thickness variations of the WPSH, IOSH, and AC circles represent the variation in intensity of the circulation systems, and the size variations of the sw and lh arrows represent their variation in intensity.

atmosphere is very complex; the relationship between SST and atmosphere is influenced not only by the variation of SST, but also the atmospheric conditions, so it is seen that the leading time shows significant interannual variation; it is not stable every year (Fig. 3). Future work is needed for improving the understanding of the response time. In addition, more research is needed to further understand the interactions and processes underlying the BoBSM onset. For example, Mao and Wu (2007) have indicated that the interannual variation in the BoBSM onset dates are significantly correlated with El Niño–Southern Oscillation (ENSO) events. Does ENSO therefore affect the interannual variation of SWSSTA occurrence through its influence on SST variability? This is one key question that needs to be addressed in the future.

Acknowledgments. This study was supported by the SOA Program on Global Change and Air–Sea Interactions (GASI-IPOVAI-03), the National Natural Science Foundation of China (Grants 41105061 and 41375110), and the State Key Program of National Natural Science of China (Grant 41530424). We sincerely thank three anonymous reviewers whose comments improved the paper.

REFERENCES

Behringer, D. W., M. Ji, and A. Leetmaa, 1998: An improved coupled model for ENSO prediction and implications for ocean initialization. Part I: The ocean data assimilation system. *Mon. Wea. Rev.*, **126**, 1013–1021, doi:10.1175/1520-0493(1998)126<1013:AICMFE>2.0.CO;2.

Chen, Y., Y. Ding, Z. Xiao, and H. Yan, 2006: The impact of water vapor transport on the summer monsoon onset and abnormal rainfall over Yunnan province in May (in Chinese). *Chin. J. Atmos. Sci.*, **30**, 25–37.

Derber, J., and A. Rosati, 1989: A global oceanic data assimilation system. *J. Phys. Oceanogr.*, **19**, 1333–1347, doi:10.1175/1520-0485(1989)019<1333:AGODAS>2.0.CO;2.

Fan, C., J. Wang, and J. Song, 2010: Factors influencing the climatological mixed layer depth in the South China Sea: Numerical simulations. *Chin. J. Oceanol. Limnol.*, **28**, 1112–1118, doi:10.1007/s00343-010-0002-6.

Fu, X., J.-Y. Lee, B. Wang, W. Wang, and F. Vitart, 2013: Intraseasonal forecasting of the Asian summer monsoon in four operational and research models. *J. Climate*, **26**, 4186–4203, doi:10.1175/JCLI-D-12-00252.1.

Gill, A. E., 1980: Some simple solutions for heat-induced tropical circulation. *Quart. J. Roy. Meteor. Soc.*, **106**, 447–462, doi:10.1002/qj.49710644905.

He, H., J. W. McGinnis, Z. Song, and M. Yanai, 1987: Onset of the Asian summer monsoon in 1979 and the effect of the Tibetan Plateau. *Mon. Wea. Rev.*, **115**, 1966–1995, doi:10.1175/1520-0493(1987)115<1966:OOTASM>2.0.CO;2.

Huang, B. Y., Y. Xue, D. X. Zhang, A. Kumar, and M. J. McPhaden, 2010: The NCEP GODAS ocean analysis of the tropical Pacific mixed layer heat budget on seasonal to interannual time scales. *J. Climate*, **23**, 4901–4925, doi:10.1175/2010JCLI3373.1.

Jian, M., H. Luo, and Y. Qiao, 2004: Seasonal variability of atmospheric heat sources over the Asian–Australian monsoon region (in Chinese). *Acta Sci. Nat. Univ. Sunyatseni*, **43**, 106–109.

Jiang, X., 2011: Air–sea interactions during monsoon onset over the Bay of Bengal. Ph.D. dissertation, Lanzhou University, 136 pp.

——, and J. P. Li, 2011: Influence of the annual cycle of sea surface temperature on the monsoon onset. *J. Geophys. Res.*, **116**, D10105, doi:10.1029/2010JD015236.

——, S. Yang, Y. Li, A. Kumar, X. Liu, Z. Zuo, and B. Jha, 2013a: Seasonal-to-interannual prediction of the Asian summer monsoon in the NCEP Climate Forecast System version 2. *J. Climate*, **26**, 3708–3727, doi:10.1175/JCLI-D-12-00437.1.

——, ——, ——, ——, W. Wang, and Z. Gao, 2013b: Dynamical prediction of the East Asian winter monsoon by the NCEP Climate Forecast System. *J. Geophys. Res. Atmos.*, **118**, 1312–1328, doi:10.1002/jgrd.50193.

Kalnay, E., and Coauthors, 1996: The NCEP/NCAR 40-year reanalysis project. *Bull. Amer. Meteor. Soc.*, **77**, 437–471, doi:10.1175/1520-0477(1996)077<0437:TNYRP>2.0.CO;2.

Kumar, S. P., and J. Narvekar, 2005: Seasonal variability of the mixed layer in the central Arabian Sea and its implication on nutrients and primary productivity. *Deep-Sea Res. II*, **52**, 1848–1861, doi:10.1016/j.dsr2.2005.06.002.

Lan, G., Z. Wen, and H. He, 2005: Comparison of the atmospheric heat sources obtained from ERA and those from NCEP2 and study of the variations in the nature of heating over the global atmosphere (in Chinese). *Chin. J. Atmos. Sci.*, **29**, 154–163.

Li, J. P., and J. Chou, 1998: The qualitative theory on the dynamical equations of atmospheric motion and its applications (in Chinese). *Chin. J. Atmos. Sci.*, **22**, 348–360.

——, and L. Zhang, 2009: Wind onset and withdrawal of Asian summer monsoon and their simulated performance in AMIP models. *Climate Dyn.*, **32**, 935–968, doi:10.1007/s00382-008-0465-8.

Li, K., W. Yu, T. Li, V. Murty, S. Khokiattiwong, T. Adi, and S. Budi, 2013: Structures and mechanisms of the first-branch northward-propagating intraseasonal oscillation over the tropical Indian Ocean. *Climate Dyn.*, **40**, 1707–1720, doi:10.1007/s00382-012-1492-z.

——, Y. Liu, Y. Yang, Z. Li, B. Liu, L. Xue, and W. Yu, 2015: Possible role of pre-monsoon sea surface warming in driving the summer monsoon onset over the Bay of Bengal. *Climate Dyn.*, doi:10.1007/s00382-015-2867-8, in press.

Liebmann, B., and C. A. Smith, 1996: Description of a complete (interpolated) outgoing longwave radiation dataset. *Bull. Amer. Meteor. Soc.*, **77**, 1275–1277.

Liu, Y., J. C. Chan, J. Mao, and G. Wu, 2002: The role of Bay of Bengal convection in the onset of the 1998 South China Sea summer monsoon. *Mon. Wea. Rev.*, **130**, 2731–2744, doi:10.1175/1520-0493(2002)130<2731:TROBOB>2.0.CO;2.

Lorenz, E. N., 1955: Available potential energy and the maintenance of the general circulation. *Tellus*, **7A**, 157–167, doi:10.1111/j.2153-3490.1955.tb01148.x.

Mao, J., 2002: Study on modal variation of subtropical high and its mechanism during seasonal transition. Part II: Seasonal transition index over Asian monsoon region (in Chinese). *Acta Meteor. Sin.*, **60**, 409–420.

——, and G. Wu, 2007: Interannual variability in the onset of the summer monsoon over the Eastern Bay of Bengal. *Theor. Appl. Climatol.*, **89**, 155–170, doi:10.1007/s00704-006-0265-1.

——, ——, and Y. Liu, 2002: Study on modal variation of subtropical high and its mechanism during seasonal transition. Part I: Climatological features of subtropical high structure. *Acta Meteor. Sin.*, **60**, 400–408.

Matsuno, T., 1966: Quasi-geostrophic motions in the equatorial area. *J. Meteor. Soc. Japan*, **44**, 25–43.

McPhaden, M. J., and S. P. Hayes, 1991: On the variability of winds, sea-surface temperature, and surface-layer heat-content in the western equatorial Pacific. *J. Geophys. Res.*, **96**, 3331–3342, doi:10.1029/90JC01726.

Qian, Y., Q. Zhang, Y. Yao, and X. Zhang, 2002: Seasonal variation and heat preference of the South Asia high. *Adv. Atmos. Sci.*, **19**, 821–836, doi:10.1007/s00376-002-0047-3.

Reynolds, R. W., T. M. Smith, C. Liu, D. B. Chelton, K. S. Casey, and M. G. Schlax, 2007: Daily high-resolution-blended analyses for sea surface temperature. *J. Climate*, **20**, 5473–5496, doi:10.1175/2007JCLI1824.1.

Roxy, M., and Y. Tanimoto, 2007: Role of SST over the Indian Ocean in influencing the intraseasonal variability of the Indian summer monsoon. *J. Meteor. Soc. Japan*, **85**, 349–358, doi:10.2151/jmsj.85.349.

——, ——, B. Preethi, P. Terray, and R. Krishnan, 2013: Intraseasonal SST–precipitation relationship and its spatial variability over the tropical summer monsoon region. *Climate Dyn.*, **41**, 45–61, doi:10.1007/s00382-012-1547-1.

Tamura, T., and T. Koike, 2010: Role of convective heating in the seasonal evolution of the Asian summer monsoon. *J. Geophys. Res.*, **115**, D14103, doi:10.1029/2009JD013418.

Wang, B., and LinHo, 2002: Rainy season of the Asian–Pacific summer monsoon. *J. Climate*, **15**, 386–398, doi:10.1175/1520-0442(2002)015<0386:RSOTAP>2.0.CO;2.

Wang, S., and Y. Qian, 2000: Diagnostic study of apparent heat sources and moisture sinks in the South China Sea and its adjacent areas during the onset of 1998 SCS monsoon. *Adv. Atmos. Sci.*, **17**, 285–298, doi:10.1007/s00376-000-0010-0.

Webster, P. J., 1972: Response of the tropical atmosphere to local, steady forcing. *Mon. Wea. Rev.*, **100**, 518–541, doi:10.1175/1520-0493(1972)100<0518:ROTTAT>2.3.CO;2.

——, V. O. Magana, T. Palmer, J. Shukla, R. Tomas, M. Yanai, and T. Yasunari, 1998: Monsoons: Processes, predictability, and the prospects for prediction. *J. Geophys. Res.*, **103**, 14 451–14 510, doi:10.1029/97JC02719.

Wu, G., and Y. Zhang, 1998: Tibetan Plateau forcing and the timing of the monsoon onset over South Asia and the South China Sea. *Mon. Wea. Rev.*, **126**, 913–927, doi:10.1175/1520-0493(1998)126<0913:TPFATT>2.0.CO;2.

——, Y. Guan, T. Wang, Y. Liu, J. Yan, and J. Mao, 2010: Vortex genesis over the Bay of Bengal in spring and its role in the onset of the Asian summer monsoon (in Chinese). *Sci. China Earth Sci.*, **40**, 1459–1467.

——, ——, Y. Liu, J. Yan, and J. Mao, 2012: Air–sea interaction and formation of the Asian summer monsoon onset vortex over the Bay of Bengal. *Climate Dyn.*, **38**, 261–279, doi:10.1007/s00382-010-0978-9.

Xie, P., and P. A. Arkin, 1997: Global precipitation: A 17-year monthly analysis based on gauge observations, satellite estimates, and numerical model outputs. *Bull. Amer. Meteor. Soc.*, **78**, 2539–2558, doi:10.1175/1520-0477(1997)078<2539:GPAYMA>2.0.CO;2.

Xing, N., J. P. Li, and Y. Li, 2014: Response of the tropical atmosphere to isolated equatorial asymmetric heating (in Chinese). *Chin. J. Atmos. Sci.*, **38**, 1147–1158.

Yan, H., Z. Xiao, and L. Wang, 2003: Activities of Bay of Bengal monsoon and beginning date of rain season in Yunnan (in Chinese). *Plateau Meteor.*, **22**, 624–630.

Yanai, M., and T. Tomita, 1998: Seasonal and interannual variability of atmospheric heat sources and moisture sinks as determined from NCEP–NCAR reanalysis. *J. Climate*, **11**, 463–482, doi:10.1175/1520-0442(1998)011<0463:SAIVOA>2.0.CO;2.

——, S. Esbensen, and J.-H. Chu, 1973: Determination of bulk properties of tropical cloud clusters from large-scale heat and moisture budgets. *J. Atmos. Sci.*, **30**, 611–627, doi:10.1175/1520-0469(1973)030<0611:DOBPOT>2.0.CO;2.

——, C. F. Li, and Z. S. Song, 1992: Seasonal heating of the Tibetan Plateau and its effects on the evolution of the Asian summer monsoon. *J. Meteor. Soc. Japan*, **70**, 319–351.

Yu, L., and R. A. Weller, 2007: Objectively analyzed air–sea heat fluxes for the global ice-free oceans (1981–2005). *Bull. Amer. Meteor. Soc.*, **88**, 527–539, doi:10.1175/BAMS-88-4-527.

——, X. Jin, and R. A. Weller, 2008: Multidecade global flux datasets from the Objectively Analyzed Air–Sea Fluxes (OAFlux) project: Latent and sensible heat fluxes, ocean evaporation, and related surface meteorological variables. Woods Hole Oceanographic Institution OAFlux project Tech. Rep. OA-2008-01, 64 pp. [Available online at http://oaflux.whoi.edu/pdfs/OAFlux_TechReport_3rd_release.pdf.]

Yu, W., J. Shi, and L. Liu, 2012: The onset of the monsoon over the Bay of Bengal: The observed common features for 2008–2011. *Atmos. Oceanic Sci. Lett.*, **5**, 314–318, doi:10.1080/16742834.2012.11447009.

Zhan, R., J. P. Li, and J. He, 2005: Statistical characteristics of the double ridges of subtropical high in the Northern Hemisphere. *Chin. Sci. Bull.*, **50**, 2336–2341, doi:10.1007/BF03183745.

Zhou, L., and R. Murtugudde, 2014: Impact of northward-propagating intraseasonal variability on the onset of Indian summer monsoon. *J. Climate*, **27**, 126–139, doi:10.1175/JCLI-D-13-00214.1.